



Saltwater flushing by freshwater in a laboratory beach

Ali Abdollahi-Nasab^a, Michel C. Boufadel^a, Hailong Li^{a,c,*}, James W. Weaver^b

^a Dept. of Civil and Environmental Engineering, Temple University, 1947 N. 12th Street, Philadelphia, PA 19122, USA

^b National Exposure Research Lab., US EPA, Athens, GA, USA

^c School of Water Resources and Environmental Science, China University of Geosciences-Beijing, Beijing 100083, PR China

ARTICLE INFO

Article history:

Received 3 April 2009

Received in revised form 1 October 2009

Accepted 3 December 2009

This manuscript was handled by P. Baveye, Editor-in-Chief

Keywords:

Density effect

Freshwater/saltwater interface

Saltwater flushing by freshwater

Laboratory beach

MARUN numerical model

SUMMARY

Experiments were conducted to investigate the flushing of saltwater out of a laboratory aquifer (or beach) by freshwater propagating seaward. After a steady state distribution was achieved with a seaward hydraulic gradient, freshwater was introduced while keeping the total head constant at each boundary. This caused the propagation of freshwater seaward. Two initial uniform concentrations were used: Case 1: 2.0 g/L (low salinity case) and Case 2: 34.0 g/L (high salinity case). The observed salinity and pressure data were closely reproduced using the MARUN (Boufadel et al. 1999a) numerical code.

The results indicated that buoyancy plays an important role for Case 2 but is negligible for Case 1. The results also indicated that the flow in the offshore beach aquifer (submerged portion of beach) was negligible especially for Case 2. For this case, the pressure increased with time until reaching a peak and then decreased (i.e., humps were formed). This was not observed in the low salinity case. Investigations revealed that the increase in pressure is due to a combination of remnant high salinity and a rise in the water table at that location. Numerical investigations revealed that for the same difference in total head, the seaward flow of freshwater increases with a decrease in the seawater salinity. The increase, however, was nonlinear as a function of seawater density. For example, the discharge in the high salinity case was 20% lower than that in the low salinity case.

© 2009 Published by Elsevier B.V.

Introduction

Seawater intrusion is a major concern for various coastal communities. The steady state interface of freshwater/seawater has been studied by many researchers in the context of saltwater intrusion in aquifers. W. Ghyben and A. Herzberg (Freeze and Cherry, 1979, p. 376) assumed static equilibrium and a hydrostatic pressure distribution in the freshwater region with stationary sea water. Glover (1959) assumed that freshwater and saltwater are at the dynamic equilibrium which is more physical. Henry (1964) developed the first analytical solution for predicting the steady state salt distribution in a confined coastal aquifer while accounting for mechanical dispersion, which results in a gradual change of the salinity between the seawater and the freshwater, a more realistic situation. However, he used a constant dispersion coefficient in his study. Frind (1982) in his finite element model considered a velocity-dependent dispersion coefficient and discussed the errors caused by use of a constant dispersion coefficient. Huyakorn

et al. (1987) presented an improved finite element model capable of simulating multiple aquifer systems, the top aquifer being confined or phreatic. Galeati et al. (1992) used an implicit Eulerian–Lagrangian finite element formulation to study the effect of dewatering on seawater intrusion through an unconfined coastal aquifer. They also discussed the effect of aquifer heterogeneity and the construction of a cutoff well on seawater intrusion. Croucher and O'Sullivan (1995) discussed the previous solutions of the Henry problem and gave possible reasons for the observed disagreements between them. They suggested that the usage of relatively few grid points could have resulted in excessive numerical dispersion that affected the numerical results. More recently, Simpson and Clement (2003) assessed the worthiness of the Henry's problem using a coupled versus uncoupled strategy. They concluded that the distribution of the saline water in Henry's problem is dictated by the boundary forcing. Consequently, Simpson and Clement (2004) presented an improved version of Henry's problem by decreasing the freshwater recharge.

All these studies addressed the steady state distribution of the saltwater in a beach aquifer. However, there are situations where knowledge of salinity evolution with time within an aquifer is essential. Examples include freshwater entering a coastal aquifer following a storm or due to seasonal variation of freshwater recharge. The evolution of salinity with time has important implica-

* Corresponding author. Address: School of Water Resources and Environmental Science, China University of Geosciences-Beijing, 29 Xue Yuan Road, Haidian District, Beijing 100083, PR China. Tel.: +1 215 204 7802; fax: +1 215 204 4696.

E-mail addresses: abdollahi@temple.edu (A. Abdollahi-Nasab), boufadel@temple.edu (M.C. Boufadel), hailongji@cugb.edu.cn, hailong@graduate.hku.hk (H. Li), Weaver.Jim@epamail.epa.gov (J.W. Weaver).

tions to biochemical reactions in coastal aquifers due to ion exchange, whereby the ions Na^+ and Mg^{2+} get replaced by Ca^{2+} when freshwater displaces saltwater in a coastal aquifer (Slomp and Van Capellen, 2004). An important application of geochemical reactions was noted by Michael et al. (2005) who provided an explanation for the high concentrations of ^{226}Ra in the southeastern US coast reported by Moore (1996).

This paper investigates the process of saltwater flushing by freshwater in a laboratory setup. Although guidelines for scaling up were presented in prior works (Boufadel et al., 1999a; Boufadel, 2000; Li et al., 2008), the investigation herein is focused on fundamental processes.

The layout of the paper is as follows: The experimental setup is presented followed by a description of the governing equations. The experimental results are then reported followed by a calibration of the numerical model MARUN (Boufadel et al., 1999a). The major factors affecting the mechanisms of transport are then investigated numerically.

Materials and methods

Facility and devices

The laboratory tank consisted of an 8 m long, 2 m high, and 0.6 m wide carbon steel tank as shown in Fig. 1. The sand in the tank was graded at a slope of 10% from a height of 1.15 m down to 0.65 m and then let to rest at its natural slope from 0.65 m to zero (the tank bottom). This resulted in a horizontal length of the beach of 6.3 m at the bottom (Fig. 1). The sand was separated from the left tank by a screen made of fine mesh. The pores of the screen were large enough (0.1 mm) to allow unhindered passage of water through them. To simulate inland freshwater recharge and concentration landward of the beach, water was pumped into the tank through a 30 cm-long manifold placed across the bottom of the left tank. A mixer was placed in the open water at the right-hand side to guarantee a uniform salt concentration in the sea. The sand used in the experiments was artificial sand composed mostly of silica (SiO_2) from Sidley, Inc., Cleveland, Ohio. It had a median size of 1.0 mm and a very narrow particle size distribution, varying between 0.8 and 1.2 mm. The particle shape was classified as “round to semiangular.” The sand porosity was determined to be 0.38, by filling a 4 L beaker with well-drained sand and adding a sufficient amount of water to produce ponding conditions at the sand surface. The ratio of the volume of the added water to the apparent volume of the sand is, by definition, the porosity of the medium. The porosity of sand in the tank was measured in situ by observing the settlement of the beach sand profile that occurred a few days after the sand was placed in the tank and covered with water. The reduction in sand height in the beach was about 4%, resulting

in a porosity of $(1-0.04)(0.38) = 0.365$. A value of 0.36 was adopted to be used in the model. The values for unsaturated flow parameters and the saturated hydraulic conductivity used by Boufadel (2000) were used as initial estimates and new values were obtained upon calibration of the model to data.

Measuring devices

The water pressure at the tank bottom was measured using Pressure Transducers (PT, model 1151AP, Fisher Scientific, Hampton, New Hampshire) that have a reading accuracy of ~ 2.0 mm of freshwater. Although the PTs were placed 3.0 cm above the bottom of the tank (Table 2 and Fig. 1), the readings were calibrated by taking the tank bottom as the datum. The Strawberry Tree data software (Strawberry Software Inc., Sunnyvale, California) was used to log and control the inflow and outflow pumps, which regulated the water flows and levels in the left and right tanks. The salt concentration was obtained through Conductivity Meters (CM) that measure the electrical conductivity of the water solution, which were calibrated to the salt concentration. The CMs were in the shape of a hollow disk (doughnut) which had the dimensions 10 cm (external diameter), 2.5 cm (internal diameter), and 3 cm (thickness). Early experimentation revealed that the Conductivity Meters were accurate within 1%. However, they were logged to a CR10 data logging software (Rocktest Inc., Plattsburg, NY) that was sensitive to power fluctuations causing a degeneration of the accuracy to about 5%. The locations of the Conductivity Meter centers are given in Table 2 and also plotted in Fig. 1. The data from all sensors were logged at an interval of 30 s. The data were collected for 16 h for the low salinity case (Case 1) and 24 h for the high salinity case (Case 2).

MARUN model

The marine unsaturated (MARUN) is a finite element model that can simulate water flows in the saturated and the unsaturated zones of two-dimensional porous media taking into account the effects of salt concentration on water density and water viscosity. Neglecting the elastic storage of the matrix, the water flow equation for homogeneous, isotropic two-dimensional domains can be written as (Boufadel et al., 1999a; Boufadel, 2000):

$$\beta\phi \frac{\partial S}{\partial t} + \beta S_0 S \frac{\partial \psi}{\partial t} + \phi S \frac{\partial \beta}{\partial t} = \frac{\partial}{\partial x} \left(\beta \delta k_r K_0 \frac{\partial \psi}{\partial x} \right) + \frac{\partial}{\partial z} \left[\beta \delta k_r K_0 \left(\frac{\partial \psi}{\partial z} + \beta \right) \right], \quad (1a)$$

where ψ (L) is the pressure head, ϕ is the porosity, S_0 (L^{-1}) is the specific storage per unit fluid weight, S is the degree of water saturation (fraction of pore volume occupied by water), K_0 (L T^{-1}) is the saturated hydraulic conductivity for freshwater (constant), k_r is the relative permeability, β is the density ratio defined as:

$$\beta = \frac{\rho}{\rho_0} = 1 + \varepsilon c \geq 1, \quad (1b)$$

where ρ (ML^{-3}) is the density of the beach pore water, $\rho_0 = 998.2 \text{ kg m}^{-3}$ is the fresh water density at 20°C , ε is a constant given in Table 1, c is the salt concentration (ML^{-3}) of the beach pore water, and δ is the dynamic viscosity ratio defined by Boufadel et al. (1999a) as:

$$\delta = \frac{\mu_0}{\mu} = 1 - \xi c \leq 1, \quad (1c)$$

where μ ($\text{ML}^{-1} \text{T}^{-1}$) is the dynamic viscosity of the beach pore water, $\mu_0 = 0.001 \text{ kg m}^{-1} \text{ s}^{-1}$ is the dynamic viscosity of the fresh water at 20°C , and ξ is a constant equal to $1.566 \times 10^{-3} \text{ m}^3 \text{ kg}^{-1}$.

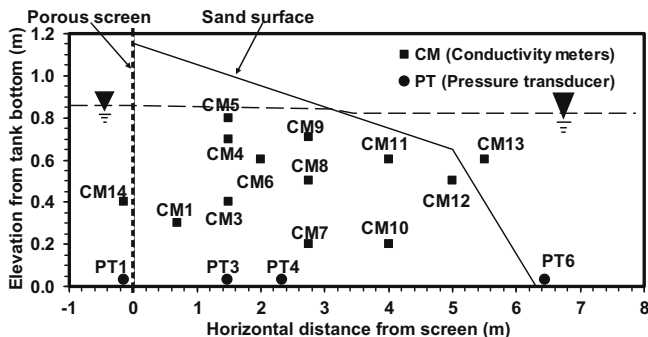


Fig. 1. Schematic of the laboratory beach and location of sensors (Conductivity Meters and Pressure Transducers). The sensor locations are given in Table 1.

Table 1
Comparison of model parameters and their values reported by Boufadel (2000) and used in the numerical simulations.

Symbol	Definition	Dimension	Reported by Boufadel (2000)	Used in this study
α	Parameter of the Van Genuchten (1980) model	1/m	12.5	18.5
n	Parameter of the Van Genuchten (1980) model	–	3.5	4.1
α_L	Longitudinal dispersivity	m	0.0075	0.0085
α_T	Transverse dispersivity	m	0.0025	0.002
ε	Fitting parameter of density-concentration relationship	m ³ /kg	7.44×10^{-4}	7.44×10^{-4}
K_0	Saturated hydraulic conductivity for freshwater	m/s	0.0075	0.0084
S_0	Specific storability	m	0.0	0.0
S_r	Residual soil saturation	–	0.01	0.01
ϕ	Sand porosity	–	0.36	0.36
CONVP	The convergence criterion of pressure head in the Picard iterative scheme of MARUN code	m	10^{-5}	10^{-5}
τ, D_m	Product of tortuosity and diffusion coefficient	m ² /s	10^{-10}	10^{-10}

Table 2
Locations of pressure and concentration sensors^a.

Sensor	x (cm)	z (cm)	y (cm)
PT1	–15	3	60
PT3	147	3	60
PT4	232.5	3	60
PT6	645	3	60
CM1	70	30	20
CM3	150	40	20
CM4	150	70	40
CM5	150	80	25
CM6	200	60	30
CM7	275	20	40
CM8	275	50	20
CM9	275	71	25
CM10	400	20	20
CM11	400	60	40
CM12	500	50	30
CM13 ^b	550	60	30
CM14 ^b	–15	40	30

^a Here, x is the horizontal distance from the screen (positive seaward), z is the elevation from the tank bottom, and y is the horizontal distance from the plexiglass wall (positive inward perpendicular to the plane of Fig. 1).

^b The sensor is in open water (see Fig. 1).

The soil moisture ratio and the relative permeability are correlated by the Van Genuchten (1980) model:

$$\text{For } \psi \geq 0: S = 1.0, k_r = 1, \quad (1d)$$

$$\text{For } \psi < 0, k_r = \sqrt{S_e} [1 - (1 - S_e^{1/m})^m]^2, \quad (1e)$$

where S_e is the effective saturation ratio given by:

$$S_e = \frac{S - S_r}{1 - S_r} = \left[\frac{1}{1 + (\alpha|\psi|)^n} \right]^m, \quad (1f)$$

where $m = 1 - \frac{1}{n}$, S_r is the residual saturation, α (L⁻¹) represents the characteristic pore-size of the beach soil, and higher α values imply a coarser material. The inverse of α provides an estimate of the capillary fringe (zone of considerable moisture above the water table). The term n represents the uniformity of the pores and higher values of n imply a more uniform pore-size distribution (Van Genuchten, 1980).

The solute transport equation used is the well-known convection–dispersion equation. In the absence of source/sink term, it can be written as (Boufadel et al., 1999a; Boufadel, 2000):

$$\phi S \frac{\partial C}{\partial t} = \beta [\nabla \cdot (\phi S \tau D_m \nabla c) + \nabla \cdot (D \nabla c)] - \mathbf{q} \cdot \nabla c, \quad (2a)$$

where $\nabla = (\frac{\partial}{\partial x}, \frac{\partial}{\partial z})$ is the gradient operator with respect to the spatial variables, $\mathbf{q} = (q_x, q_z)$ (L T⁻¹) is the Darcy flux vector defined as:

$$\mathbf{q} = (q_x, q_z) = -\delta k_r K_0 \left(\frac{\partial \psi}{\partial x}, \frac{\partial \psi}{\partial z} + \beta \right), \quad (2b)$$

the term τ (dimensionless) is the domain tortuosity, D_m (L² T⁻¹) is the diffusion coefficient (molecular diffusion). The term D in (2a) represents the dispersion tensor given by

$$D = \frac{1}{\|\mathbf{q}\|} \begin{pmatrix} \alpha_L q_x^2 + \alpha_T q_z^2 & (\alpha_L - \alpha_T) q_x q_z \\ (\alpha_L - \alpha_T) q_x q_z & \alpha_T q_x^2 + \alpha_L q_z^2 \end{pmatrix}, \quad (2c)$$

where $\|\mathbf{q}\| = \sqrt{q_x^2 + q_z^2}$, α_L (L) and α_T (L) are the longitudinal and transverse dispersivities, respectively (Bear, 1972, pp. 614–615).

The governing Eqs. (1) and (2) used in MARUN are designated as density-and-viscosity-dependent flows in two-dimensional variably saturated media. The equations are discretized in space by the standard Galerkin method, and integrated in time using backward Euler with mass lumping (Celia et al., 1990). The MARUN code has been used to reproduce previous well-known numerical results such as the Henry's problem of seawater intrusion (Boufadel et al., 1999a,b; Croucher and O'Sullivan, 1995; Frind, 1982), and the Elder problem (Boufadel et al., 1999b; Elder, 1967).

Experimental and numerical approach

Two experiments (Cases 1 and 2) were designed and conducted to investigate the density effect on beach groundwater flow and solute transport paths. The maximum change of the solute (salt) concentration was 2.0 g/L for Case 1 and 34.0 g/L for Case 2. The salt in Case 1 acts as a tracer, as the numerical simulations revealed. The salinity variation of Case 2 was chosen to represent typical salinity variation on beaches at the coasts of the continental United States. The salt used in the experiments was a commercial grade of sodium chloride (NaCl).

Experiment

Prior to each of the experiments the tank was filled with salt water and was circulated through the tank until a uniform salt concentration was reached. Then, while conserving the same concentration for the corresponding case, the pressures at sensors PT1 and PT6 were set equal to 0.857 m and 0.831 m, respectively.

Each experiment started by introducing fresh water (tap water) to the left of the screen through the same manifold used to introduce salt water under the same constant-pressure boundary conditions. Because of the difference in water head between PT1 and PT6, the fresh water propagated in the beach toward the sea side, causing a reduction of the salinity in the beach. Fresh water was pumped through the manifold to the left tank whenever the reading at PT1 dropped by more than 0.2 cm below the design value of 0.857 m, and the pumping stopped whenever the reading at PT1 increased by more than 0.2 cm above the design value. The converse occurred at the right tank, where the mixed water was pumped out whenever the reading at PT6 increased by more than 0.2 cm above the design value of 0.831 m.

The open water levels on the left- and right-hand side boundaries were controlled by the readings at PT1 and PT6. The fluctuations of the pressure readings at PT1 and PT6 resulted from two reasons. The first reason was that 2 mm in pressure drop at PT1 were needed to activate the freshwater pump to introduce water into the left tank. The similar was true in the right tank where an increase of water level by 2 mm was needed to activate the outflow pump. The second reason for the fluctuations in the readings is due to voltage fluctuation in the data collection software.

The injected fresh water contained air bubbles, which increased the mixing in the open water in the left tank. The air bubbles rose vertically and there was no indication that they passed through the fine mesh screen and entered the sand. Salinity measurements at different heights to the left of the screen indicated that the open water there, was well mixed. Therefore, the reading at CM14 can represent the concentration left boundary condition.

Modeling

The mesh contained 46,965 nodes and 92,736 triangular elements; the spacing between nodes varied from 1.25 cm to 0.5 cm, being largest at $x=0, z=0$ and smallest at $x=5\text{ m}, z=0.65\text{ m}$. The time steps for the numerical simulation were 15 s. The convergence criterion of pressure head for the Picard iterative scheme of MARUN code was $CONVP = 10^{-5}\text{ m}$ (Table 1).

Boundary conditions. For the flow equation at the screen ($x=0$), a Dirichlet boundary condition below the water level (in the open water of the left tank) is:

$$\psi(0, z) = H(PT1) - z[1 + \epsilon c(CM14)], \tag{3a}$$

where $H(PT1)$ is the PT1 reading in meters of freshwater, $c(CM14)$ is the concentration of CM14, ϵ is the parameter in Eq. (1b), and c is the salt concentration expressed in grams of salt per liter of solu-

tion. Eq. (3a) represents a hydrostatic pressure distribution for $\psi(0, z) \geq 0$ in the saturated zone. For $\psi(0, z) < 0$ (the unsaturated zone above the water level in the tank) a no-flow Neumann boundary condition ($\frac{\partial \psi}{\partial n}|_{x=0} = 0$) was assigned.

On the right and upper boundaries which represent the beach surface, a Dirichlet boundary condition was used:

$$\psi(x, z) = H(PT6) - z[1 + \epsilon c(CM13)], \text{ if } \psi(0, z) > 0. \tag{3b}$$

As the seepage face observed in the experiment was only 4 cm, smaller than the horizontal mesh size, it was not modeled in the simulations.

For salt concentration at $x=0$ and the beach surface, for $\psi(0, z) \leq 0$ (on the beach surface higher than the right water level including the seepage face), $\frac{\partial c}{\partial n}|_{x=0} = 0$ (Neuman). For $\psi(0, z) > 0$ (boundary submerged by the open water) a Dirichlet boundary condition was assigned with $c(0, z) = c(CM14)$ at $x=0$ and $c(x, z) = c(CM13)$ on the beach surface. This boundary condition is discussed further by Boufadel et al. (1999a).

Initial conditions. The initial pressure head and concentration distributions were obtained by running the MARUN model from an approximate initial condition until steady state was achieved. The water levels in the left and right tanks were $\frac{0.857}{1+\epsilon c}$ m and $\frac{0.831}{1+\epsilon c}$ m, respectively. The concentration throughout the tank was equal to 2.0 g/L for Case 1 and 34.0 g/L for Case 2.

Results and discussion

Experimental results

The observed concentrations and pressure heads are presented in Figs. 2 and 3 for low and high salinity cases, respectively. Fig. 2a shows how the observed concentrations dropped with time for

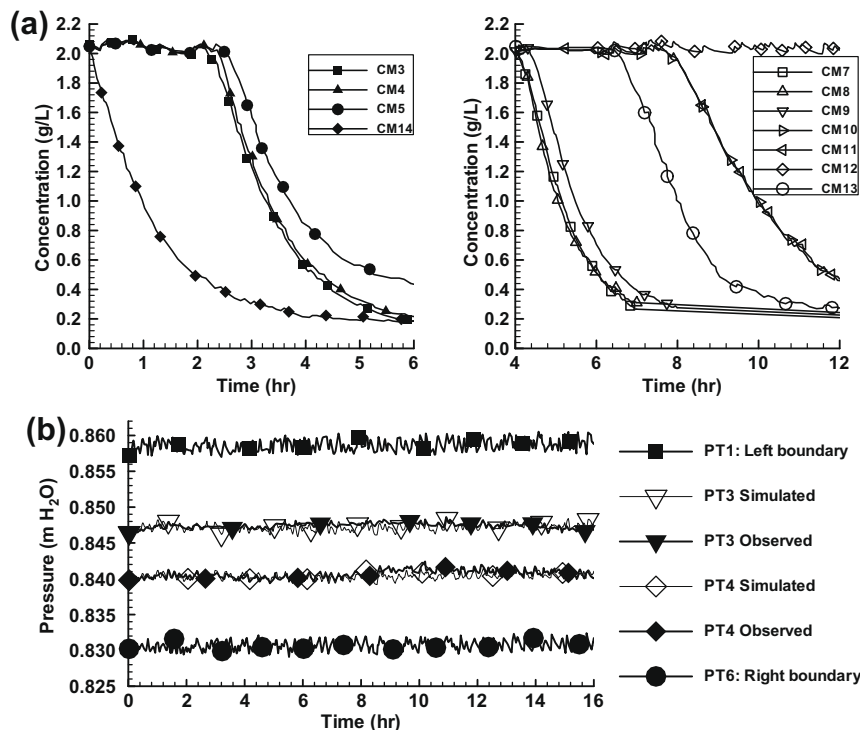


Fig. 2. (a) Observed concentration dropping with time for Case 1 (low salinity case) at three groups of Conductivity Meters {CM3, CM4, CM5, CM14}, {CM7, CM8, CM9}, and {CM10, CM11, CM12, CM13}. Readings at CM13 and CM14 served as the right and left boundary conditions for concentration, respectively. (b) Simulated versus observed pressures at four Pressure Transducers (PT1, PT3, PT4, and PT6) for Case 1 (low salinity case). The pressure head at each Pressure Transducer was calibrated by taking the tank bottom as the datum.

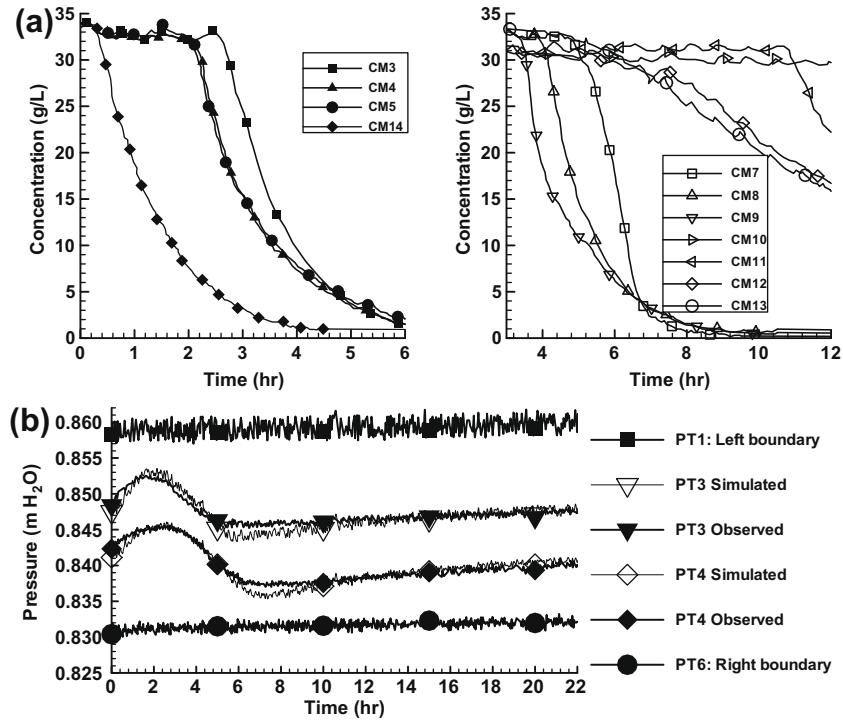


Fig. 3. (a) Observed concentration dropping with time for Case 2 (high salinity case) at three groups of Conductivity Meters (CM3, CM4, CM5), (CM7, CM8, CM9), and (CM10, CM11, CM12, CM13). Readings at CM13 and CM14 served as the right and left boundary conditions for concentration, respectively. (b) Simulated versus observed pressures at four Pressure Transducers (PT1, PT3, PT4, and PT6) for Case 2 (high salinity case). The pressure head at each Pressure Transducer was calibrated by taking the tank bottom as the datum.

Case 1 (low salinity case) at three groups of Conductivity Meters {CM3, CM4, CM5}, {CM7, CM8, CM9}, and {CM10, CM11, CM12, CM13}. The first two sensor groups are located onshore and the third, offshore. In addition, sensors in each of the first two groups have the same *x*-coordinates.

In Fig. 2a, the time order for the fresh water front to arrive at the sensors is: $CM3 \leq CM4 < CM5$, $CM8 \approx CM7 < CM9$. The readings at CM3 and CM4 were very close, so were those at CM7 and CM8, indicating a freshwater front moving seaward that is almost vertical. The delay of CM5 and CM9 is due to the proximity of the upper sensors to the water table, where the unsaturated zone filled with saltwater initially acted as a source of salt, causing a sustained high value of salinity near the water table.

Fig. 3a shows how the observed concentrations decreased with time for Case 2 (high salinity case) at three groups of Conductivity Meters {CM3, CM4, CM5}, {CM7, CM8, CM9}, and {CM10, CM11, CM12, CM13}. The time order for the fresh water front to arrive at the sensors in Fig. 3a is almost reversed compared with that in Fig. 2a: $CM5 \leq CM4 < CM3$, $CM9 < CM8 < CM7$, indicating buoyancy effect where the light freshwater occupied the top portion of the beach and is underlain by the heavier saltwater.

It is also important to observe that, for both low and high salinity cases, the readings at CM10 and CM11, which were offshore dropped much slower than those at CM9 and CM13 (open water on the right-hand side). This indicates that fresh water leaves the beach near the coastline, and only a very small horizontal (seaward) flow occurs seaward of that point. This was supported by visual observation, through the transparent wall of the tank, of sand erosion (due to high flow) that occurred only around the coastline. The erosion of the sand was on the order of 0.5 cm in elevation (5 cm in horizontal length).

Because a constant concentration in the sea was not achievable experimentally, the concentration in the sea decreased due to dilution by the incoming freshwater. However, this did not affect the

concentration in the beach significantly because the flow velocity in the offshore beach (i.e., seaward of the water line) was much smaller than that in the onshore beach.

The pressures at PT3 and PT4 for the high salinity case (Fig. 3b) behaved very differently from the low salinity case (Fig. 2b). While the pressures at PT1 and PT6 were constant (by design), the pressures at PT3 and PT4 exhibited strong variations of about 0.5 cm, which were large considering that the pressure head difference across the beach is only $(85.7 - 83.1) = 2.6$ cm (freshwater column). These “humps” were the result of the continuous introduction of the freshwater plume in the tank behind the screen under constant pressure at PT1. In fact, the introduction of freshwater in the tank will lead to the increase of the water level there, because the water density drops while the pressure at PT1 remains practically constant (not accounting for the fluctuations). The initial water level equals $\frac{85.7}{1+6c} = 83.6$ cm, where $c = 34.0$ g/L, and the final water level equals 85.7 cm (when there is only freshwater in the tank). Thus, the total water level increase in the left tank during the experiment is about 2.1 cm. The increase of the water level in the left tank caused the diluted water to enter the beach above the existing water table, while the pore water below the water table was still at the high initial concentration of about 34.0 g/L. This explains why the readings at PT3 and PT4 rose during the initial stage of the experiment. The decrease in the readings at PT3 and PT4 after the initial rise is due to the decrease in the density, because the salinity of the pore water above the transducers was replaced with freshwater when the freshwater front moved seaward. This fact can be verified from the readings of PT3 (in Fig. 3b), CM3, CM4, and CM5 (in Fig. 3a), which are located approximately at the same vertical cross section. After $t = 5$ h, the salinity at CM3, CM4, and CM5 became essentially negligible (less than 4.0 g/L) in Fig. 3a, and the reading at PT3 stopped dropping in Fig. 3b. The reading at PT4 stopped dropping at about $t = 6$ h (Fig. 3b), indicating that the

salinity in the pore water above PT4 became negligible after about 6 h of the experiment. The pressure hump is investigated in detail later using numerical simulations.

Numerical modeling

A good overall fit was achieved between the simulated and the observed pressures and concentrations, as shown in Figs. 2b and 4 (Case 1), and Figs. 3b and 5 (Case2). The parameters' values are reported in Table 1 which shows that they are close to those obtained by Boufadel (2000) (see Fig. 5).

Fig. 6 shows the simulated spatial distribution of concentration and the Darcy flux at two times, $t = 4$ h and 8 h, for the low salinity

case (Case 1). The freshwater seems to propagate seaward as a vertical front in the beach, except near the water table, where the contours become more curved. This is consistent with measurements, where the observed delay of the concentration decreases at CM5 with respect to CM3 and CM4, and at CM9 with respect to CM7 and CM8 (Fig. 2a). This indicates that neglecting unsaturated flow in modeling would result in an erroneous solute distribution near the water table.

The large magnitude of the Darcy flux around the water line (i.e., the intersection point of the water table and the beach surface) shows that most of the water leaves the beach around that location. This also explains why the concentration at CM13 (open water on the right-hand side) decreased to about 1.0 g/L at

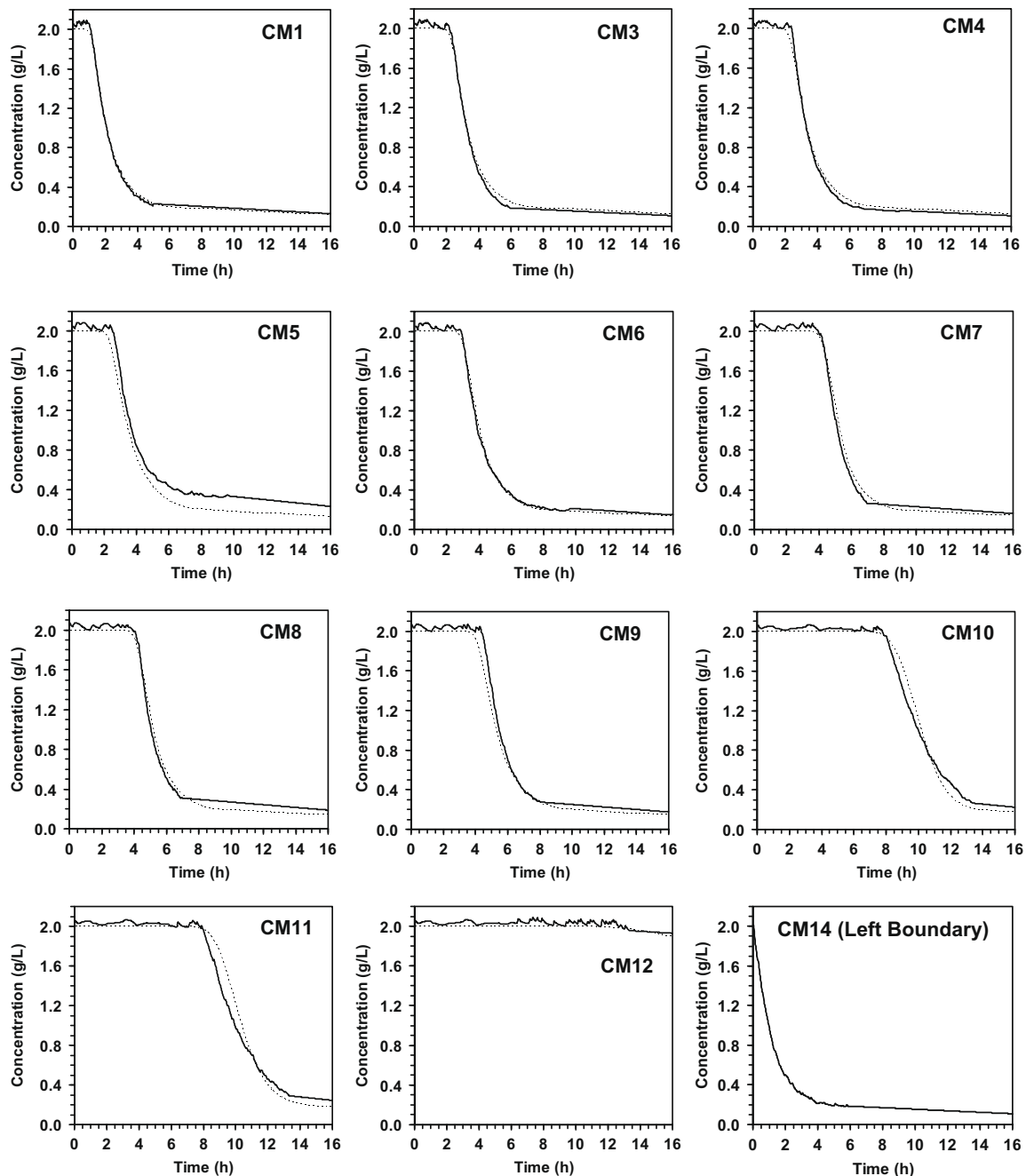


Fig. 4. Simulated versus observed concentrations at 12 Conductivity Meters (CM1, CM3, ..., CM12, and CM14) for Case 1 (low salinity case). The dashed lines in the concentration figures are the simulation results.

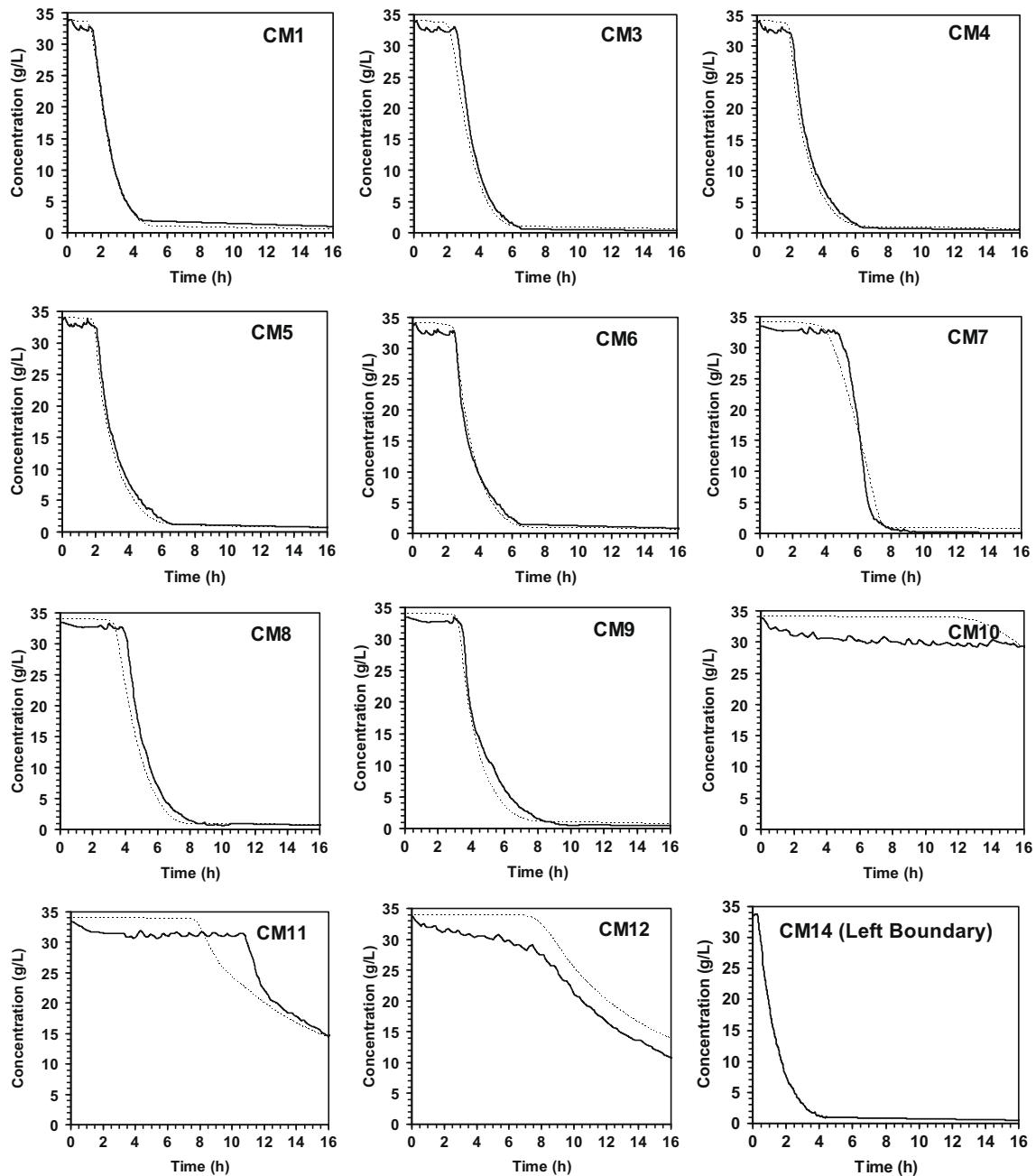


Fig. 5. Simulated versus observed concentrations at 12 Conductivity Meters (CM1, CM3, ..., CM12, and CM14) for Case 2 (high salinity case). The dashed lines in the concentration figures are the simulation results.

$t = 8$ h, while the concentration at CM10, CM11, and CM12 were still at their maximum (initial) values (Fig. 2a). The significant reduction of the Darcy flux seaward of the exit point occurs because the total head in that region is almost uniform, as imposed by the open water above it. Thus, water leaving the beach would take the shortest path, which is upward instead seaward where there is more resistance through the sand.

Fig. 7 shows the spatial distribution of concentration and the Darcy flux at two times, $t = 4$ h and 8 h, for the high salinity case (Case 2). The salinity distribution in Fig. 7 is very different from that in Fig. 6; the development of the freshwater/saltwater interface in Fig. 7 is much clearer than that in Fig. 6 and a clear salt wedge was formed at the bottom of the domain for the high salinity case. Interestingly, the effect of buoyancy seems to be stronger during transient regime ($t = 4.0$ h) in comparison with the steady

state ($t = 8.0$ h and larger). The diffuse saltwater wedge was much larger at $t = 4.0$ h, indicating that neglecting buoyancy effects at that time would result in a higher error than neglecting it at steady state.

For all cases, the velocity vectors landward of the exit point (coastline) are at least one order of magnitude greater than those seaward of the exit point. This indicates a very limited flow in the offshore beach aquifer, which acts approximately as an impermeable zone for the seaward flow forcing the water to move more upward towards the beach surface near the coastline.

To investigate the behavior of the freshwater front in Case 2 as it propagated seaward, we focused on the vertical cross section passed through PT3. Fig. 8 shows how the pressure head and the concentration changes with time at four elevations located on that cross section. The pressure head at $z = 0.836$ m increased from neg-

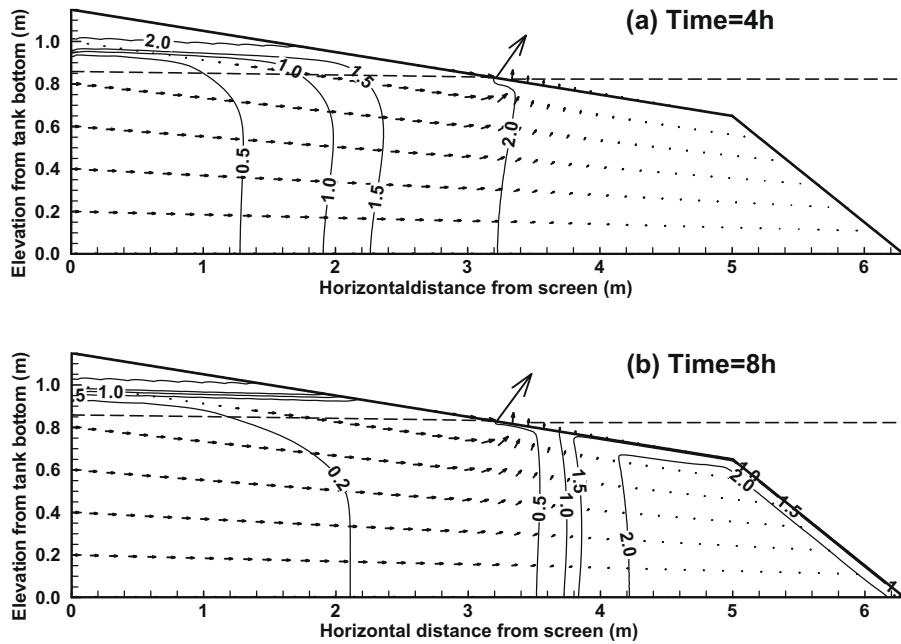


Fig. 6. Simulated concentration contours (in g/L), Darcy velocity field (arrows), and water table or open water level (dashed lines) for Case 1 (low salinity case) at (a) $t = 4$ h and (b) $t = 8$ h.

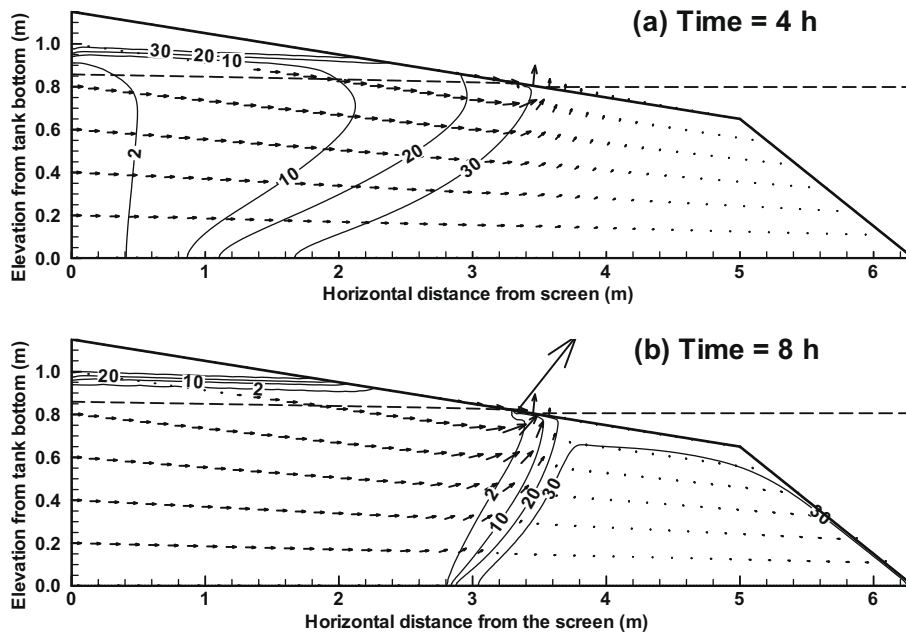


Fig. 7. Simulated concentration contours (in g/L), Darcy velocity field (arrows), and water table or open water level (dashed lines) for Case 2 (high salinity case) at (a) $t = 4$ h and (b) $t = 8$ h. Buoyancy effects are noted, especially at early time ($t = 4$ h).

ative values to become positive as the concentration decreased, indicating that the pore space at that location was unsaturated (with water) before the freshwater front arrived and the water table rose. The pressure variation range was greatest at $z = 0.836$ m (about 2.0 cm), and decreased with depth, reaching about 0.5 cm at the bottom. As the depth increases, the pressure increase caused by the rising water table was counteracted by the pressure decrease caused by the decrease in density, and resulted in the smallest variation range of about 0.5 cm.

It can be also observed from Fig. 8 that the lower the elevation, the later the arrival time of the freshwater front (the time when the

concentration drops). This is due to the buoyancy effect which will be detailed in the following subsection. The pressure head at a given point in the absence of the vertical flow depends on the water density and depth of the saturated pore water above it. When the freshwater front was propagating seaward the density decreased, but the depth of the saturated pore water increased due to the rising of the water table. The decrease in density tends to decrease the pressure head, while the rising of the water table tends to increase it. At the highest point ($z = 0.836$ m), the depth of the saturated pore water is zero, or very small. In this case, the pressure head is not influenced by dropping of the density, and it increases

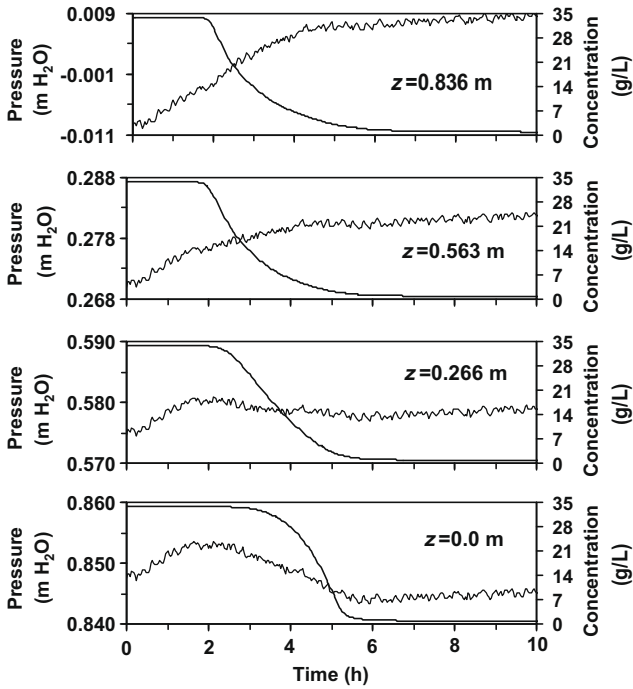


Fig. 8. Variations of pressure head (thin solid lines) and concentration (thick solid lines) with time at different elevations of $z = 0.0$ m, 0.266 m, 0.563 m, and 0.836 m (from bottom to top) along the vertical cross section passed through PT3 ($x = 1.47$ m) for Case 2 (high salinity case).

with rising of the water table. At the bottom of the tank ($z = 0.0$ m), the depth of the saturated pore water is the greatest. In this case the pressure is influenced by both the decrease of the density and the rise of the water table.

Fig. 9 reports the water table, pressure head and the average concentration which changes with time at the vertical cross section passed through PT3. At the initial stage ($t = 3.5$ h) the water table rose, but the density remained unchanged or decreased only within the upper small portion of the cross section, so the pressure increased. When most of the freshwater front passed the cross section ($t \approx 6$ h), the rate of rising of the water table became slow, while the density decreased in most of the cross section so that

the pressure stopped increasing and then began decreasing. This clearly explains the reason for forming the pressure humps.

Fig. 10 shows the distributions of concentration, and horizontal and vertical Darcy velocities along the vertical cross section passed through PT3 at different times of $t = 0.0$ h, 2.2 h, 4.3 h, 5.5 h, and 6.3 h for Case 2. At the initial time, the concentration is uniform along the cross section, there is no vertical flow ($V_z = 0.0$ m/d), and the horizontal Darcy flux is also uniform in the saturated portion (approximately when $z < 0.825$ m). When $t = 2.2$ h, the concentration began dropping at a position located just below the water table. The horizontal Darcy flux reached its maximum value near the water table and decreased with depth. Considerable vertical Darcy flux occurred (although it is at least one order of magnitude smaller than the horizontal one). The negative V_z value indicates that the flow is downward, which was caused by the freshwater flushing over the original saltwater water table. As time elapsed, the drop in concentration occurs at points farther below the water table, and finally concentration became uniformly negligible in the saturated zone. The horizontal Darcy flux is highest at the water table when the freshwater front passed the cross section, and tended to be uniform in the saturated zone after the freshwater front passed the cross section. The most interesting phenomenon is the behavior of the vertical Darcy flux. It was downward (indicated by negative value of V_z) when $t = 2.2$ h, and became positive in the middle-elevation zone when $t = 4.3$ h and 5.5 h. This was caused by the decrease of the concentration (density) in the middle zone while the concentration at bottom of the tank remained significantly high. It finally tended toward zero as the concentration at the tank bottom also approached zero, as illustrated by the figure when $t = 6.3$ h. In the unsaturated zone, due to low water saturation, the Darcy flux was essentially zero and the concentration remained at the initial value (maximum concentration).

Idealized scenarios

An idealized scenario was designed to investigate how the velocity of salinity dropping at the left tank affects the pressure “hump”. In this scenario it was assumed that the concentration at the left tank drops from its maximum value (34 g/L) to zero instantaneously, after 1 h, 2 h and 4 h (Fig. 11a). Fig. 11b and c show the effect of time lag on the pressure head at a vertical cross section passed through PT3 and PT4, respectively. The maximum pressure value is decreasing as the time lag increases for both PT3 and PT4. However, the difference between the maximum pres-

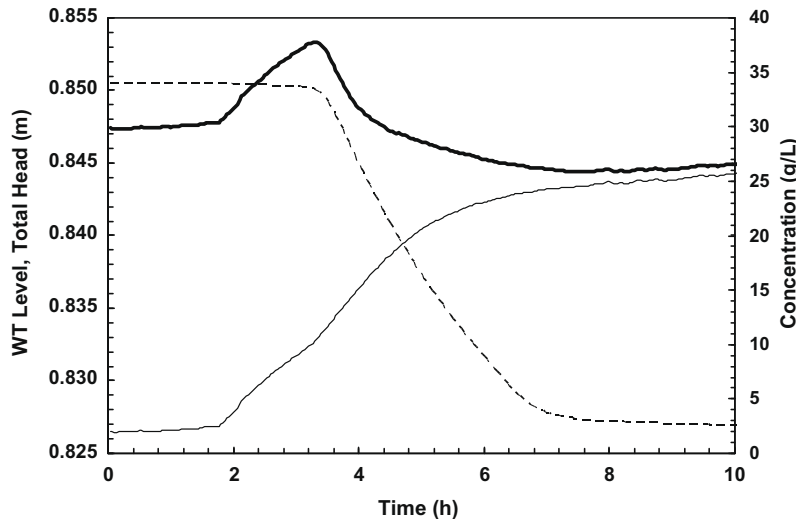


Fig. 9. Variations of pressure head (thick solid line), water table (thin solid line), and average concentration (thin dashed line) with time along the vertical cross section passed through PT3 ($x = 1.47$ m) for Case 2 (high salinity case).

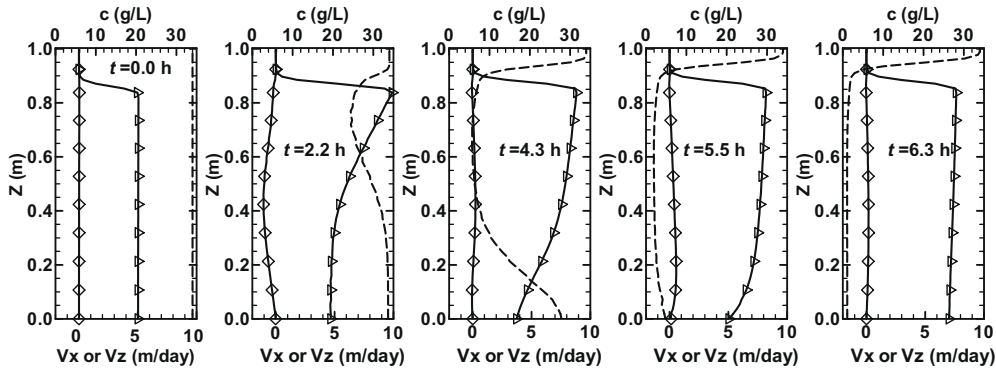


Fig. 10. Distributions of concentration (dashed lines), horizontal Darcy velocity V_x (solid lines with right triangles), and vertical Darcy velocity V_z (solid lines with diamonds) along the vertical cross section passed through PT3 at different times $t = 0.0$ h, 2.2 h, 4.3 h, 5.5 h, and 6.3 h (from left to right) for Case 2 (high salinity case).

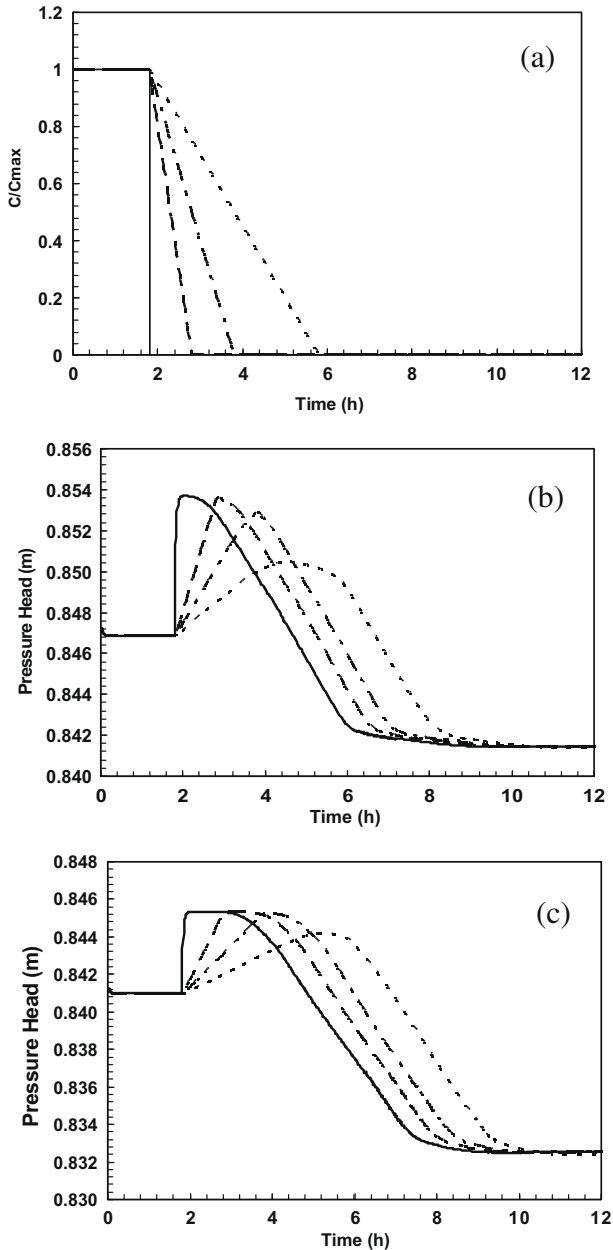


Fig. 11. Time lag graphs for (a) concentration drop at left tank, (b) pressure head at PT3, and (c) pressure head at PT4. The time lags are 0 (thick solid lines-concentration drops instantaneously), 1 h (dashed lines), 2 h (dashed-dotted lines), and 4 h (dotted lines).

sure values for two cases (no time lag and 4 h time lag) is relatively larger at PT3 compared to PT4 (Fig. 11b and c). This is because the PT3 is closer to the left tank and concentration variations play a more important role in forming the pressure hump. In other words, landward locations of the beach are more sensitive to the sudden changes in the salinity in the left tank (say freshwater recharge). This shows that in a real system, the rate that the freshwater enters a beach after a storm has influence on forming the pressure hump.

To investigate the effect of salinity on the final distribution of the salt in the beach, another idealized scenario was designed and simulated numerically. In this scenario, four values were chosen for sea water concentrations which are 2, 10, 25 and 34 g/L, and a hydraulic gradient was selected as the same for all cases.

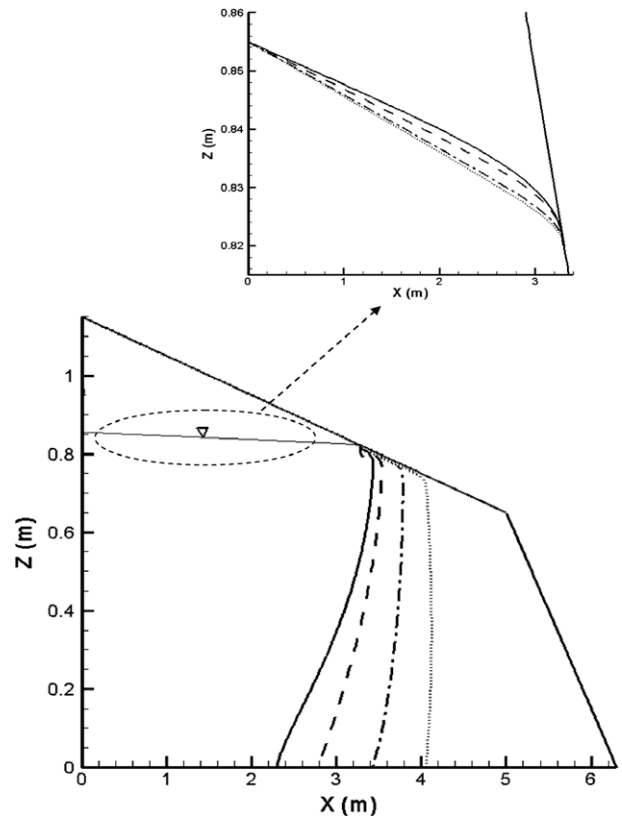


Fig. 12. Comparison of water table and freshwater/seawater interface for different seawater concentrations in the idealized case. The seawater concentrations are 34 g/L (solid lines), 25 g/L (dashed lines), 10 g/L (dashed-dotted lines), and 2 g/L (dotted lines).

To have the same hydraulic gradient, the water levels in the left tank and sea side were designed to be equal to 0.855 m and 0.820 m, respectively for all cases. The left tank was filled completely with fresh water, so its concentration is zero for the whole simulation period. Similarly, the concentration at the “sea” did not change with time. In every simulation it was assumed that the beach was filled with seawater initially, then freshwater entered from the left tank and propagated in the beach due to the hydraulic gradient. The simulations continued until the steady state situation was reached.

In Fig. 12, the water table and the freshwater/seawater interface for different cases are compared. Based on this figure, the freshwater/seawater interface moves farther seaward for the lower salinity cases. The interface shape for the high salinity case is relatively close to what can be predicted by Ghyben–Herzberg approximation (Freeze and Cherry, 1979, p. 376). Based on the Ghyben–Herzberg formula, the depth of the interface below sea level is 40 times the height of the fresh water table above it. The simulation results show that this ratio is 48 for the high salinity case. One of the main reasons for the difference between these two values is that the Ghyben–Herzberg approximation is based on a vertical sea-land interface but here the beach has only a 10% slope. Also, Ghyben–Herzberg assumed a simple case in which freshwater and seawater are at the static equilibrium, while in our simulations we were dealing with the dynamic equilibrium. For the low salinity cases, we were not able to calculate this ratio because when the difference between seawater and freshwater densities decreases, the freshwater/seawater interface becomes more vertical, and our experimental beach is not deep enough to allow us to do this calculation.

In Fig. 13 the water table differences between the low salinity case (2 g/L) and higher salinity cases are compared. Based on this figure, higher levels of seawater concentration lead to a higher water table. It is also visible in Fig. 13 that the maximum value of the water table moves farther landward as the salinity increases. It should be noted that the difference between maximum values of the water table is not proportional to the salinity difference. This reflects the highly nonlinear behavior of the system.

Fig. 14 compares the average horizontal volumetric fluxes at the vertical cross section through PT3 for different seawater concentrations. Although there is variation with time, it is not purpose of this study to compare the long term (large time) results. The seaward volumetric flux seems to decrease as the salinity increase, and the difference between the 2 g/L case and that of 34 g/L is about 20%. Using a mass flux instead of a volumetric flow rate would have decreased the difference by only 2%. Therefore, there is an-

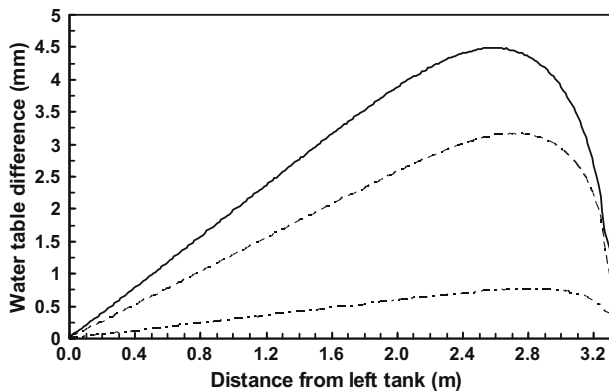


Fig. 13. Water table differences between the low salinity case (2 g/L) and higher salinity cases in the idealized scenario. The seawater concentrations for these cases are 34 g/L (solid line), 25 g/L (dashed line), and 10 g/L (dashed-dotted line).

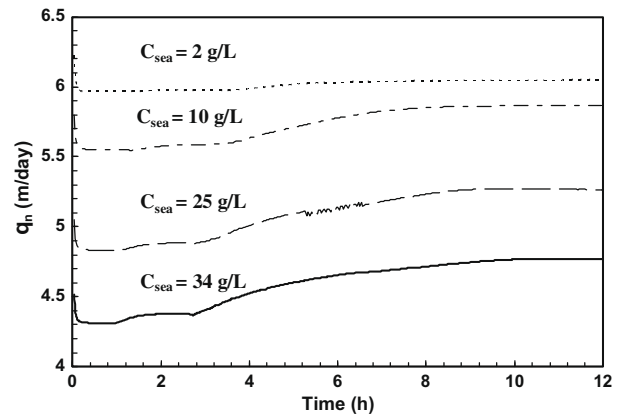


Fig. 14. Average horizontal water flux at a vertical cross section passed through PT3 for different seawater concentrations. The seawater concentrations are 34 g/L (thick solid line), 25 g/L (dashed line), 10 g/L (dashed-dotted line), and 2 g/L (dotted line).

other factor affecting the flow, the hydraulic gradient. The hydraulic gradients between the left tank and the cross section passed through PT3 were 7.52×10^{-3} for the high salinity case (34 g/L) and 9.50×10^{-3} for low salinity case (2 g/L). Thus, the hydraulic gradient for the high salinity case was almost 20% smaller than the low salinity case, which explains the difference in average flux reported in Fig. 14. Therefore, the increase in seawater density by only 2% could result in a decrease in the seaward flow rate by 20%, highlighting the nonlinear behavior of the system.

The impact of the capillarity above the water table on the pressures at PT3 and PT4 was investigated by conducting the simulation using a large α value of 92.5 m^{-1} (five fold of its normal value which corresponds to low capillarity effect), while the other parameters remained unchanged. The simulated pressures at PT3 and PT4 (not shown) provided essentially the same results with humps about 0.5 cm high, indicating that the capillarity has no effect on the forming of the pressure humps.

Summary and conclusions

Experiments were conducted to investigate the flushing of salt-water out of a laboratory aquifer (or beach) by freshwater propagating seaward. After a steady state distribution was achieved with a seaward hydraulic gradient, freshwater was introduced while keeping the bottom pressure constant, causing the propagation of freshwater. Two initial uniform concentrations were used: Case 1: 2.0 g/L (low salinity case) and Case 2: 34.0 g/L (high salinity case). The observed salinity and pressure data were closely reproduced using the MARUN numerical code (Boufadel et al., 1999a).

The results indicated that buoyancy plays an important role for Case 2 but is negligible for Case 1. The results also indicated that the flow in the offshore beach aquifer (submerged portion of beach) was negligible (low flow zone), compared to the flow in the onshore aquifer in both cases, but the difference was strikingly large for the high density case. The landward extent of the low flow zone increased with the density difference between the seawater and the inland water; it was approximately vertical for a small density difference (Case 1). For the high salinity case the pressure increased with time until reaching a peak and then decreased (i.e., humps were formed). This was not observed in the low salinity case. Further investigations indicated that the seaward propagation of the freshwater/saltwater interface resulted in the rise of the water table and a decrease of the pore water density in the saturated zone. The former tends to increase the pressure and the latter tends to decrease the pressure. However, as pressure fronts

propagate faster than concentration fronts (because the water is incompressible), an increase in pressure occurred. As the freshwater arrived at that location, the density decreased causing a reduction in pressure.

The results showed that the water table increases with an increase in the seawater salinity for fixed water levels, landward of the aquifer and at sea. The increase was found to be superlinear as a function of the seawater density, reflecting the nonlinear dynamics of the system. Also, the seaward flow of freshwater increased with a decrease in the seawater salinity, and the increase was nonlinear as function of seawater density. For example, the discharge in the high salinity case was about 20% lower than that in the low salinity case.

Our results have important implications on the dynamics of saltwater flushing and the discharge location of an aquifer to its abutting open waters, such as rivers, lakes and sea where the waves and tides are negligible. It is concluded that if the slope of the beach surface is mild below the water surface, then the inland groundwater discharge will exit around the intersection of the surfaces of the open water and the interface. This gives helpful instructions related to the sampling location of the groundwater discharge into open waters using the seepage meter (see e.g., Taniguchi et al. (2006) and references there).

Acknowledgments

Funding for this work was provided by the US Department of Environmental Protection and by the Exxon Valdez Trustee Council under Project Number 070836. However, it does not necessarily reflect the views of the Council, and no official endorsement should be inferred. This research was also partially supported by the National Natural Science Foundation of China (40672167). We are very grateful for the helpful review comments from the editor and two anonymous reviewers.

References

- Bear, J., 1972. *Dynamics of Fluids in Porous Media*. American Elsevier, New York, NY.
- Boufadel, M.C., 2000. A mechanistic study of nonlinear solute transport in a groundwater–surface water system under steady-state and transient hydraulic conditions. *Water Resources Research* 36 (9), 2549–2566.
- Boufadel, M.C., Suidan, M.T., Venosa, A.D., 1999a. A numerical model for density- and viscosity-dependent flows in two-dimensional variably-saturated porous media. *Journal of Contaminant Hydrology* 37, 1–20.
- Boufadel, M.C., Suidan, M.T., Venosa, A.D., Rauch, C.H., Bowers, M.T., 1999b. Steady seepage in trenches and dams: effect of capillary flow: application to trenches and dams. *Hydraulic Engineering* 125, 286–294.
- Celia, M.A., Bouloutas, E.T., Zarba, R.L., 1990. A general mass-conservative numerical solution for the unsaturated flow equation. *Water Resources Research* 26 (7), 1483–1496.
- Croucher, A.E., O'Sullivan, M.J., 1995. The Henry problem for saltwater intrusion. *Water Resources Research* 31 (7), 1809–1814.
- Elder, J.W., 1967. Transient convection in a porous medium. *Journal of Fluid Mechanics* 27 (3), 609–623.
- Freeze, R.A., Cherry, J.A., 1979. *Groundwater*. Prentice Hall, Englewood Cliffs, New Jersey.
- Frind, E.O., 1982. Simulation of long-term transient density-dependent transport in groundwater. *Advanced in Water Resources* 5, 73–88.
- Galeati, G., Gambolati, G., Neuman, S.P., 1992. Coupled and partially coupled Eulerian–Lagrangian model of freshwater–seawater mixing. *Water Resources Research* 28 (1), 149–165.
- Glover, R.E., 1959. The pattern of fresh water flow in coastal aquifers. *Journal of Geophysical Research* 64, 439–475.
- Henry, H.R., 1964. Effects of dispersion on salt encroachment in coastal aquifers. US Geological Survey of Water Supply Paper, c71–c84.
- Huyakorn, P.S., Mercer, J.W., Ward, D.S., 1987. Saltwater intrusion in aquifers: development and testing of a three-dimensional finite element model. *Water Resources Research* 23 (2), 293–312.
- Li, H.L., Boufadel, M.C., Weaver, J.W., 2008. Tide-induced seawater-groundwater circulation in shallow beach aquifers. *Journal of Hydrology* 352 (1–2), 211–224.
- Michael, H.A., Mulligan, A.E., Harvey, C.F., 2005. Seasonal oscillations in water exchange between aquifers and the coastal ocean. *Nature* 436, 1145–1148. doi:10.1038/nature03935.
- Moore, W.S., 1996. Large groundwater inputs to coastal waters revealed by ²²⁶Ra enrichments. *Nature* 380, 612–614.
- Simpson, M.J., Clement, T.P., 2004. Improving the worthiness of the Henry problem as a benchmark for density-dependent groundwater flow models. *Water Resources Research* 40 (1), W01504.
- Simpson, M.J., Clement, T.P., 2003. Theoretical analysis of the worthiness of the Henry and Elder problems as benchmarks of density-dependent groundwater flow models. *Advance in Water Resources* 26, 17–31.
- Slomp, C., Van Capellen, P., 2004. Nutrient inputs to the coastal ocean through submarine groundwater discharge: controls and potential impact. *Journal of Hydrology* 295, 64–86.
- Taniguchi, M., Ishitobi, T., Shimata, J., 2006. Dynamics of submarine groundwater discharge and fresh–seawater interface. *Journal of Geophysical Research* 111, C01008. doi:10.1029/2005JC002924.
- Van Genuchten, M.T., 1980. A closed-form equation for predicting the hydraulic conductivity of unsaturated soils. *Soil Science Society of America Journal* 44, 892–898.